The solid state photo-CIDNP effect

Daviso, E.

Chapter 5

GENERAL DISCUSSION AND FUTURE OUTLOOK

5.1 INTRODUCTION

In Chapter 1 the photo-CIDNP effect in solids has been explained as a combination of several mechanisms, the TSM, the DD and the DR mechanisms.

Chapter 2 describes a new laser-NMR setup for the solid state. A fiber bundle delivers laser light pulses of ~8 ns at the side of the spinning sample. The combination of periods of polarization extinction with a NMR presaturation pulse sequence and polarization generation with light pulses allows for fast NMR detection. Since the lifetime of the laser light pulse is shorter than the electron photo-cycle, the technique allows to detect primary electron-nuclear interactions. It has been demonstrated that the photo-CIDNP effect in ^{13}C labeled RCs is highly driven by spin diffusion so that under continuous illumination the nuclear polarization build-up is obscured by nuclear relaxation mechanisms.

Build up and evolution of photo-CIDNP occurring during a single photocycle in bacterial RCs of *Rb. sphaeroides* are reported in Chapter 3. Electron-nuclear and electron-electron-nuclear interactions have been simulated and the relevant magnetic parameters are discussed. In steady state experiments, nuclear polarization in generated by the TSM, DD and DR mechanisms (Table 5.1). TSM and DD are coherent mechanisms that require hyperfine anisotropy to transfer the electron polarization to nuclei. The DR is a relaxation mechanism occurring in the carotenoidless R26 RCs by selective erasing of nuclear polarization of the triplet donor induced by the fluctuation of anisotropic hyperfine fields. Under steady state conditions, the singlet and triplet polarization contributions caused by A_{zz}, cancel out. The presaturation pulse sequence has been used to perform time-resolved ns-flash photo-CIDNP MAS NMR experiments allowing to detect photochemically induced transient nuclear polarization and transiently obscured polarization in photosynthetic RCs of *Rb. sphaeroides*. The Chapter describes a new technique to measure the kinetics of the quenching of the triplet donor by the carotenoid in RCs of *Rb. sphaeroides* wild type as well as the triplet donor lifetime in R26. Furthermore, photo-CIDNP computations of the primary photosynthetic radical pair are presented.

Chapter 4 aims to resolve the electronic structures of the primary donor at atomic resolution. Time-resolved ns-flash photo-CIDNP MAS NMR allows to observe the electron densities of the ground-state that are related to the chemical shifts and the electron spin densities of the radical pair that are proportional to the NMR intensities. The photo-CIDNP intensities arising from the singlet state of R26 are proportional to a_{iso} thus to *s* spin densities. On the other hand, the photo-CIDNP intensities arising from the singlet plus triplet states are proportional to ΔA^2 thus to the square of *p* spin densities (Diller *et al.*, 2007b). In addition, density functional theory computations of hyperfine tensors are used to discuss the shift of electron spin densities towards P_L.

Mechanisms	Action	Type	Hfi
TSM	ISC	Coherent	ΔA
DD	RP decay	Coherent	a_{iso}, ΔA
DR	long living donor T	Relaxation	ΔA

Table 5.1: Mechanisms that generate photo-CIDNP, action required for occurrence of the mechanisms, type of mechanism and essential part of the hfi for the occurrence of the solid-state photo-CIDNP effect.

Observable	Kinetics	Requirements	Effect
TNP	singlet radical pair to ground state	$T_S \neq T_T$	NP singlet spin selection
TOP	excited triplet to ground state	Paramagnetic interaction	NP obscured by triplets

Table 5.2: Scheme of the transient effects observed by ns-flash photo-CIDNP MAS NMR in photosynthetic RCs, the paths of the nuclear polarization, the requirements for the occurrence of the effects and the path of the nuclear polarization.

5.2 APPLICATIONS OF NS-FLASH PHOTO-CIDNP MAS NMR

In the following I will show some examples of applications for ns-flash photo-CIDNP MAS NMR that confirm the experimental observation and the theorical model adopted in this thesis. These achievements are possible by a time-resolved approach that detects nuclear polarization generation and links it to numerical calculations. Such theoretical models can be applicable for time-resolved solid-state DNP methods as well.

5.2.1 Towards liquid state

The photo-CIDNP effect in RCs occurs in the liquid state with much less intensity than in the solid state.

The experiments in Figure 5.1 have been performed using purified RCs of *Rb. sphaeroides* R26 in the MAS NMR probe at 4 °C under the spinning speed of 1000 Hz using a spin-echo pulse sequence on the ^{13}C channel. Trace A is the spectrum collected in the dark revealing broad peaks between 0-80 ppm arising from the protein-detergent system. Trace B is the spectrum collected under continuous illumination. In the time resolved experiment in which the $\pi/2$ detection pulse follows the excitation light pulse (Trace C), photo-CIDNP intensities from the donor at about 165 ppm as well as from the acceptor at about 110 ppm become visible. The time-resolved experiment has been collected with the same number of scans of the steady state. In contrast to the solid-state, the signal intensities of the transient spectrum are stronger than with continuous illumination. A possible explanation is that the isotropic hf is dominant while anisotropic contributions may be partly averaged out by the tumbling of the protein. Further studies on the rotational correlation time and viscosity of photosynthetic RCs are needed to understand residual coupling or anisotropic averaging effects. Development of a photo-CIDNP setup at lower magnetic field, where a theoretical nuclear enhancement of a factor ~100000 has been calculated (Jeschke and Matysik, 2003), would provide more insight into the mechanisms occurring in the liquid state.

5.2.2 The electronic structure of the primary photosynthetic radical pair

The photo-CIDNP effect occurs since the magnetic parameters of the radical pair such as the electron-electron dipolar coupling, exchange coupling and hfi lie in a narrow region that is between 5 and 20 MHz (see Appendix A).

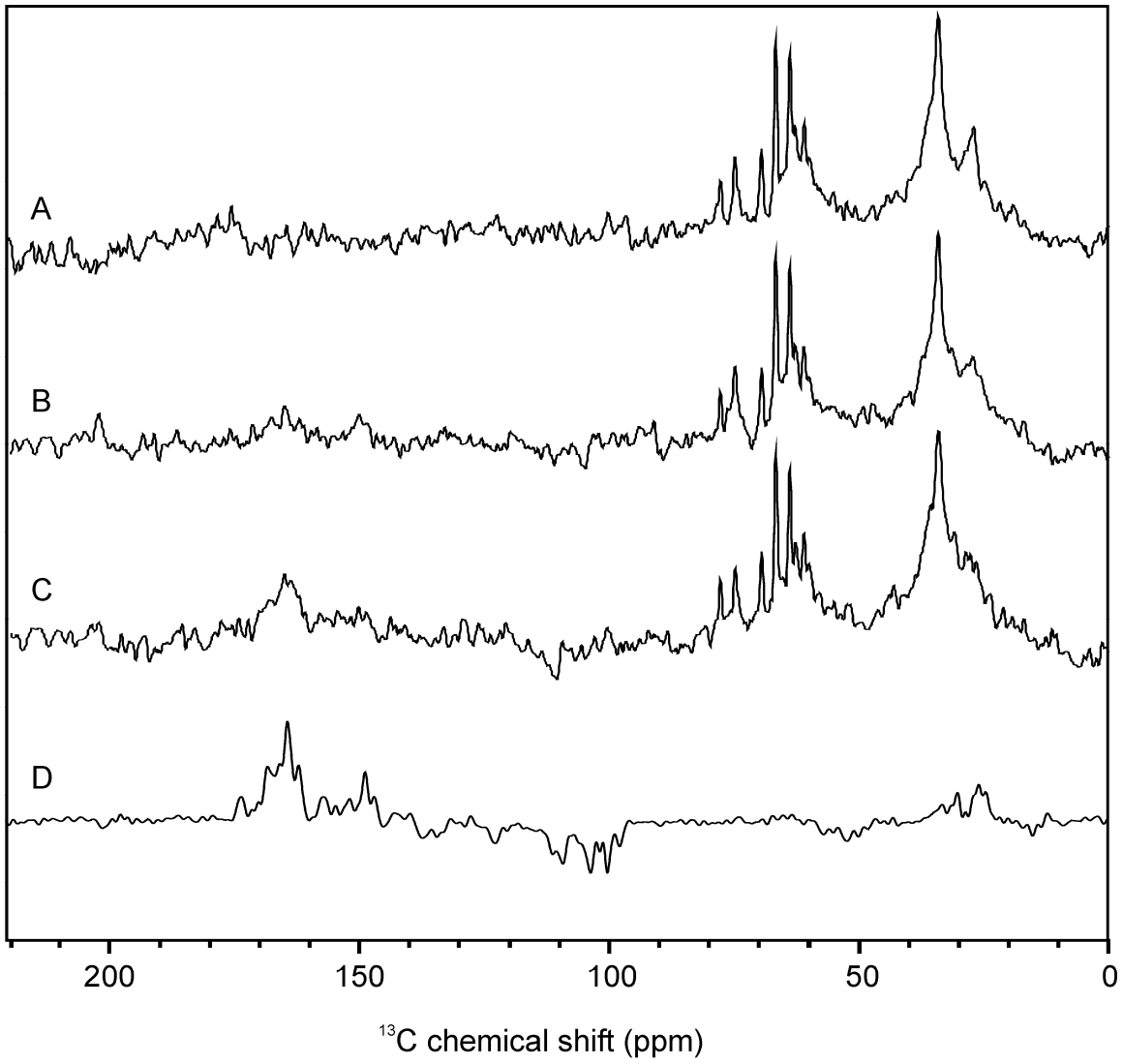

Figure 5.1: (A) Dark spectrum of purified RCs of *Rb. sphaeroides* R26. (B) Liquid state photo-CIDNP NMR spectrum collected under continuous illumination. (C) ns-flash liquid photo-CIDNP NMR collected with a delay time between light pulse and NMR detection pulse of 0 μs. All the spectra have been collected in the liquid state using a spin echo pulse sequence on the ^{13}C channel. (D) ns-flash liquid photo-CIDNP MAS NMR collected with a delay time between light pulse and NMR detection pulse of 0 μs.

I have shown in Chapter 4 that the photo-CIDNP intensities from the transient spectrum of *Rb. sphaeroides* R26 are proportional to the a_{iso} thus to the electron spin densities in *s* orbitals. In addition to this, the computed photo-CIDNP intensities arising from the singlet (see Chapter 1 and 3) are also proportional to a_{iso}.

In Figure 5.2, the map obtained from experimental transient photo-CIDNP intensities (A) matches the normalized computed photo-CIDNP intensities arising from the singlet state (B). In a similar case to Chapter 4, the two representations have been plotted by normalizing on the total volume of the spheres. In Diller *et al.* (2007b) it has been shown that the electron spin densities in *p* orbitals scale with ΔA^2 thus proportional to

the photo-CIDNP NMR intensities observed under continuous illumination from the spectrum of *Rb. sphaeroides* WT. Figure 5.2C and Figure 5.2D show respectively the experimental and the calculated photo-CIDNP intensity maps obtained from the primary photosynthetic radical pair under steady state conditions. Also in this case, the two representations have been plotted by normalizing on the total volume of the spheres. A detailed analysis is now required to correlate the ground state electron densities and the radical pair state electron spin densities to the energetic levels of the primary photosynthetic radical pair.

5.2.3 Action spectroscopy

The efficiency of charge separation can be measured by performing ns-flash photo-CIDNP experiments using different light excitation wavelengths. The coupling of an OPO to the laser permits to tune the light wavelength between 720 to 940 nm under our current experimental conditions. Even if the measured energy loss is quantified at about 70%, selectivity is increased, allowing the measurement of transient spectra.

Figure 3.8 shows the evolution of ns-flash photo-CIDNP MAS NMR spectra using excitation wavelengths of 860 nm (A), 803 nm (B) and 756 nm (C), being respectively the maximum absorption VIS-NIR of the two BChl of the primary donor, of the accessory BChls and of the bacteriopheophytins in the RCs of *Rb. sphaeroides*.

The spectral evolution from 0 to 100 μs does not change (traces red, green and dark blue) thus the TOP observed in WT (see Chapter 3) rules out a long living light induced paramagnetic state of the Car. The determination of the efficiency of charge separation is measured considering the action spectra of nuclear polarization of C-19 of P_L as a function of the wavelength (Figure 5.3). Detailed analyses of the spectra may be useful to probe optical properties as well as charge separation efficiency in photosynthetic proteins (Denblanken *et al.*, 1984).

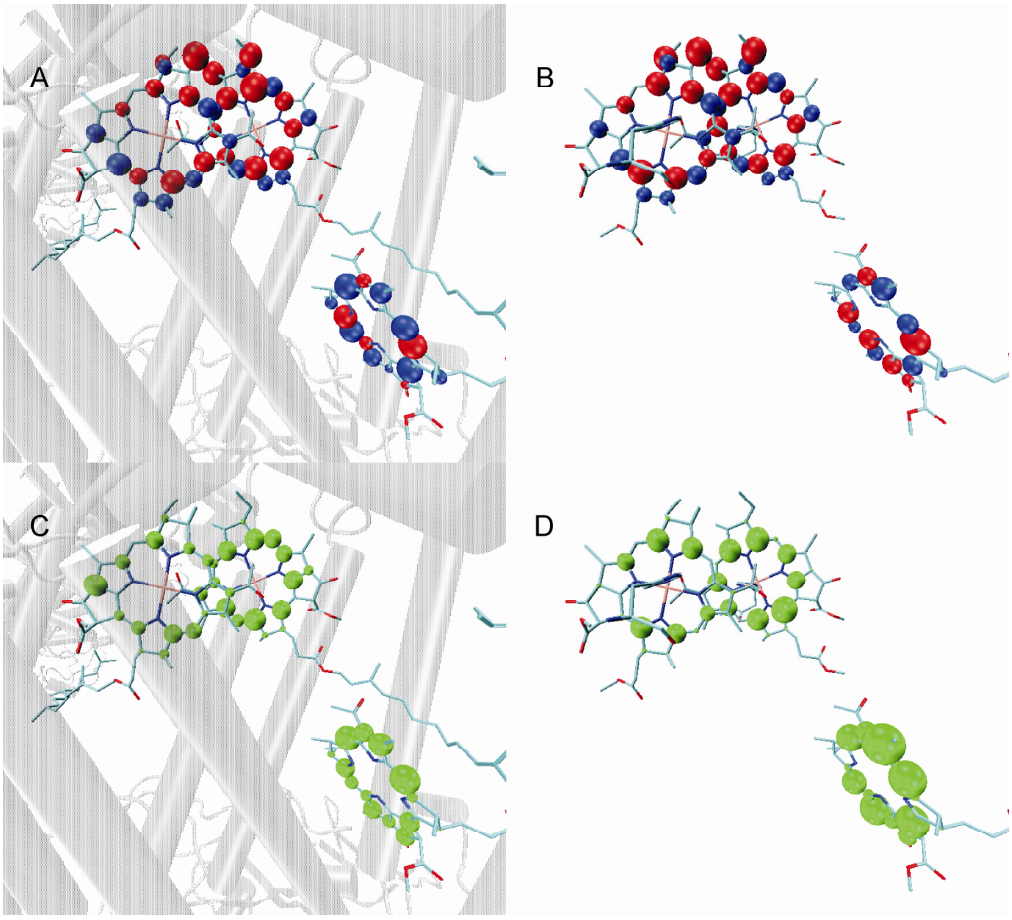

Figure 5.2: (A) Normalized fitted photo-CIDNP intensities observed from *transient* nuclear polarization at a timescale of 0 µs between light excitation and NMR detection in RCs of *Rb. sphaeroides* R26. Positive (absorptive) signals are shown in red, negative (emissive) signals are indicated by blue spheres. (B) Calculated photo-CIDNP intensities arising from the singlet. Red spheres correspond to positive isotropic hf values, while blue spheres to negative ones. (C) Normalized fitted photo-CIDNP intensities observed under *steady state* conditions in RCs of wild type. All signals are emissive and represented as green spheres. (D) Calculated photo-CIDNP intensities arising from the singlet plus triplet. The size of the green spheres scales with $-\Delta A^2$. To compare the experimental data (A-C) with the theory (B-D), nuclear polarization and calculated photo-CIDNP intensities were normalized by setting the cumulative volume of the spheres to a fixed value for optimal visualization.

5.3 FUTURE OUTLOOK

5.3.1 Ns-flash photo-CIDNP MAS NMR 2-dimensional spectroscopy

Expanding the NMR experiment to multiple dimensions will improve our knowledge of the structure of primary polarized photosynthetic radical pairs.

A 2-dimensional pulse sequence in combination with ns-flash photo-CIDNP MAS NMR would enable spin-torch experiments where the kinetic parameters of spin diffusion can be measured. In combination with continuous illumination 2-D experiments, the technique will allow a better insight into the structure of the photosynthetic active cofactors involved in the primary charge separation. Figure 5.4 is an example of a suggested RFDR ns-flash photo-CIDNP pulse sequence.

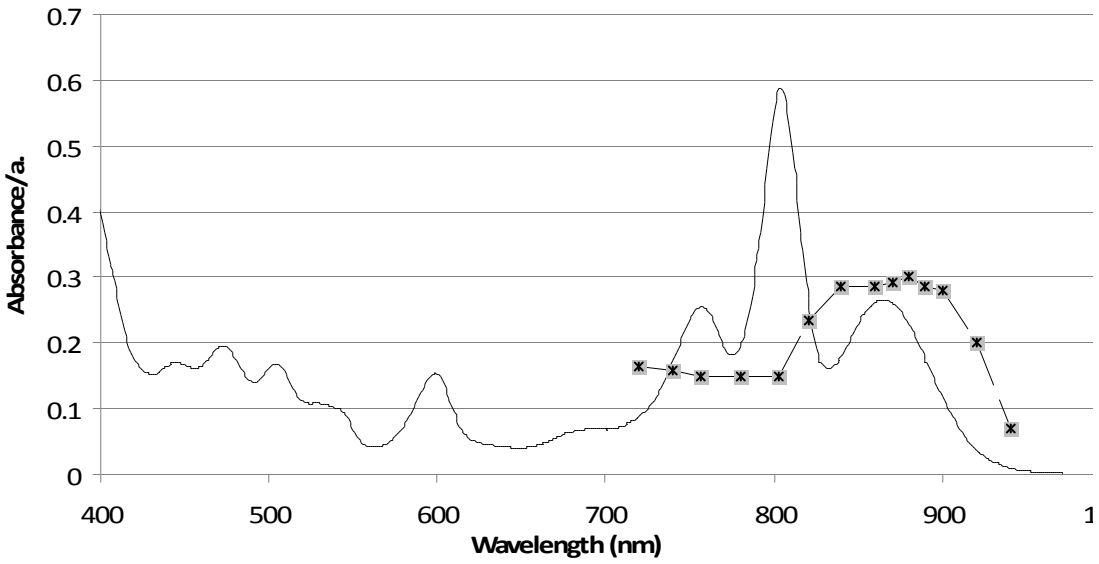

Figure 5.3: The solid line is a UV-VIS-NIR spectrum of purified RCs of *Rb. sphaeroides* wild type. The peak at 860 nm is assigned to the bacteriochlorophylls of P. The peak at 803 nm is assigned to the accessory bacteriochlorophylls. The peak at 756 nm is assigned to the bacteriopheophytins. The dashed line is the action spectrum of photo-CIDNP intensities of C-19 of P_L plotted as a function of the wavelength.

5.3.2 Labeled carotenoid in RCs

The presence of ^{13}C selectively labeled Car would allow more insight into the mechanism of primary photo-CIDNP generation as well as of nuclear-nuclear spin diffusion. The sample might be prepared either by reconstitution of labeled Car in RCs of *Rb. sphaeroides* R26 (Bautista *et al.*, 1998) or by growing *Rb. sphaeroides* WT cells with a ^{13}C labeled precursor of the biosynthesis of the spheroidene such as pyruvate (Rohmer, 1999).

5.3.3 Imaging with microstrips

Currently, sensitivity enhancement by hyperpolarization is a hot topic in NMR and MRI. Especially DNP and optical pumping receive great attention (Tycko and Reimer, 1996).

The solid-state photo-CIDNP effect, especially in conjunction with stripline-NMR (Figure 5.5), provides a serious alternative which has to be explored. The combination of the two methods would not only add the positive aspects of both methods but would improve the capacity of photo-CIDNP solid-state NMR further: (i) the small sample size provide excellent optical conditions since even in optically dense samples the light can penetrate deeply, (ii) the new type of coils allows for NMR pulses in the nanosecond range, improving dramatically the time resolution of photo-CIDNP NMR experiments.

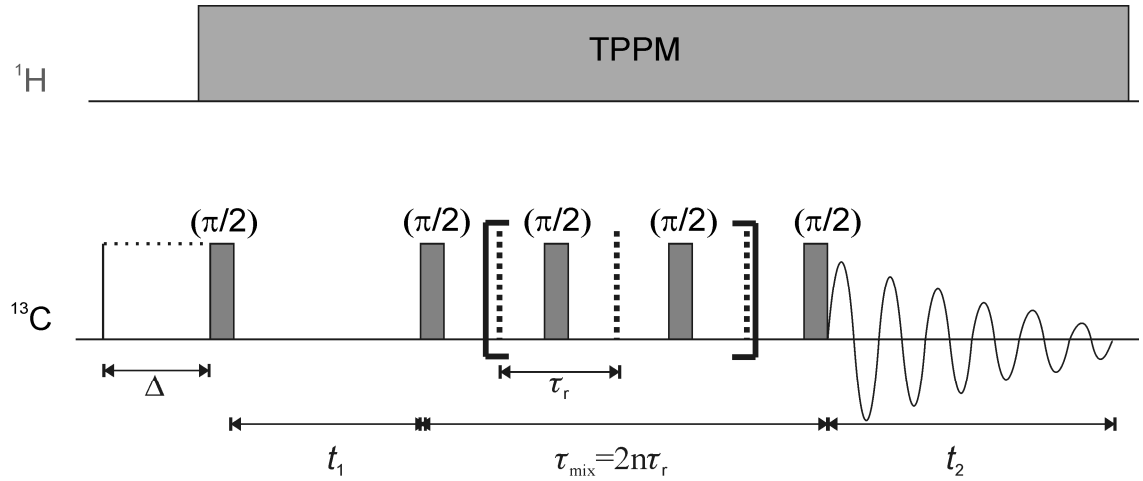

Figure 5.4: An example of a 2-dimensional NMR experiment, the ns-flash photo-CIDNP-RFDR pulse sequence. t_1 is the indirect dimension. t_2 is the direct dimension. Δ is the interpulse delay between the laser light pulse and NMR detection pulse. τ_r is one rotor period. τ_{mix} is 2n times the rotor period.

Hence, photo-CIDNP stripline NMR may provide a realistic chance to improve signal sensitivity in ^{13}C NMR and MRI. Photo-CIDNP micro-imaging NMR can be applied to investigate the organization of photosynthetic RCs in membranes and the architecture of these membranes. In particular, the heliobacterial membranes should be applied since they are simple in preparation and handling and enrichable in ^{13}C isotopes. Coating of the stripline detector with such membranes may allow for direct detection of the spatial organization of the RCs in the membrane. Such experiments will pave the way for future spin-torch experiments in which polarization of artificial RCs is used to explore properties of surfaces and cavities.

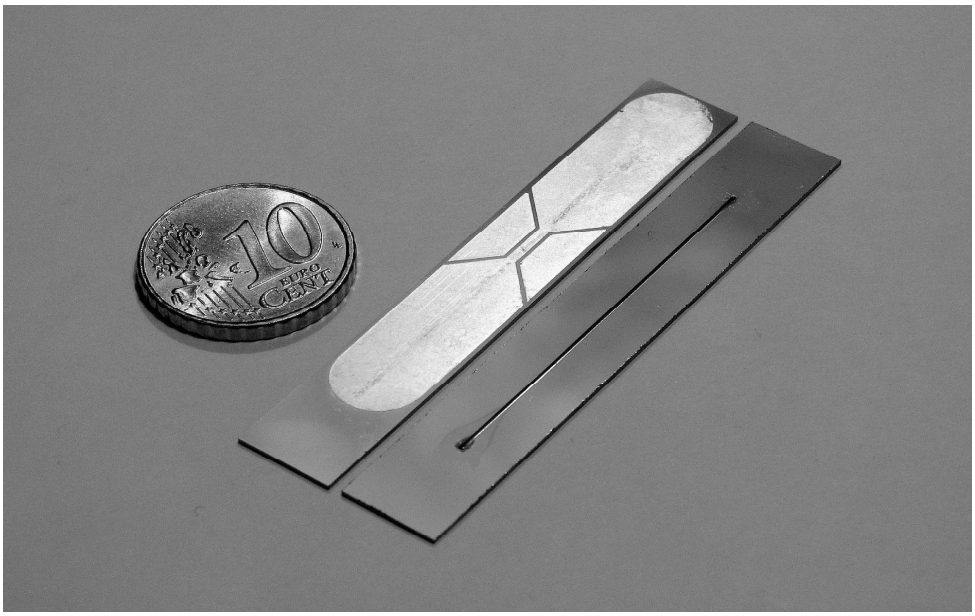

Figure 5.5: Photograph of a microfluidic NMR chip based on the stripline design.